ACI STRUCTURAL JOURNAL TECHNICAL PAPER

Title no. 102-S17

Experimental Study on Seismic Behavior of High-Performance Fiber-Reinforced Cement Composite Coupling Beams

by B. Afsin Canbolat, Gustavo J. Parra-Montesinos, and James K. Wight

Current design provisions in the ACI Building Code for reinforced concrete (RC) coupling beams in earthquake-resistant structures require substantial reinforcement detailing to ensure a stable seismic behavior, leading to reinforcement congestion and construction difficulties. As a design alternative, the use of high-performance fiber-reinforced cementitious composites (HPFRCCs) in coupling beams with a simplified reinforcement detailing was experimentally investigated. To validate this alternative, four coupling beam specimens were tested, including an RC control specimen detailed as per the 1999 ACI Building Code. A precast construction process was proposed for the HPFRCC coupling beams in this study. This construction alternative would lead to significant savings in time and workmanship at the job site, and provide good material quality control. Results from large-scale tests demonstrated the superior damage tolerance and stiffness retention capacity of HPFRCC coupling beams. It was also observed that diagonal reinforcement is necessary to achieve large displacement capacity. However, the transverse reinforcement around the diagonal bars was successfully eliminated due to the confinement provided by the HPFRCC material.

Keywords: fiber-reinforced concrete; load; shear strength; tension.

INTRODUCTION

Seismic resistance of medium-rise reinforced concrete (RC) buildings typically relies on structural walls due to their good lateral strength and stiffness properties. Architectural considerations usually result in window and door openings in structural walls, which divide a single wall into more slender walls connected by short, deep beams, referred to as coupling beams. The use of coupling beams leads to a more efficient and economical structural system than individual walls because properly designed coupled wall systems possess significantly higher strength, stiffness, and energy dissipation capacity. Thus, system efficiency and performance greatly depend on the behavior of the coupling beams under high shear reversals. Damage observed after the 1964 Alaska earthquake demonstrated the vulnerability of coupling beams to large load reversals (American Iron and Steel Institute 1975) when conventional detailing, consisting of distributed horizontal and vertical reinforcement (Fig. 1(a)), is used.

Extensive studies on the seismic behavior of coupling beams (Luisoni, Somenson, and Ungaro 1970; Paulay and Binney 1974; Paulay and Santhakumar 1976) led to the development of an improved reinforcement detailing that consists of a group of diagonal reinforcing bars within the span of the coupling beam (Fig. 1(b)). In this reinforcement detail, the diagonal bars need to be carefully anchored in the walls and confined by closely spaced transverse reinforcement, similar to that used in RC columns. In the design of this type of coupling beam, the whole shear transfer mechanism is assigned to the heavily reinforced diagonal cages. Experimental results have shown that diagonally reinforced coupling beams are capable of maintaining their shear strength with good stiffness retention and energy dissipation capacity under large displacement reversals (Paulay and Binney 1974; Shiu et al. 1978; Tassios, Moretti, and Bezas 1996; Galano and Vignoli 2000). The diagonal reinforcement detailing, however, creates construction difficulties due to the reinforcement congestion problems associated with the placement of the diagonal bars and closely spaced transverse reinforcement. These drawbacks have led to the evaluation of other reinforcement alternatives, such as the addition of dowels or diagonal reinforcement only at the beam-wall interface (Fig. 1(c) and (d)). However, for coupling beams with a span-to-depth ratio less than or equal to 2.0, diagonal reinforcement over the full beam span has been shown to be the most efficient solution (Tassios, Moretti, and Bezas 1996).

During the 1990s, developments in fiber-reinforced cementitious composites have allowed the achievement of high-performance behavior with low volume fractions ($V_f \leq 2.0\%$), resulting in new possibilities for earthquake engineering applications. High performance refers to a tensile strain-hardening behavior where the postcracking strength is larger than the first cracking strength, and is accompanied by

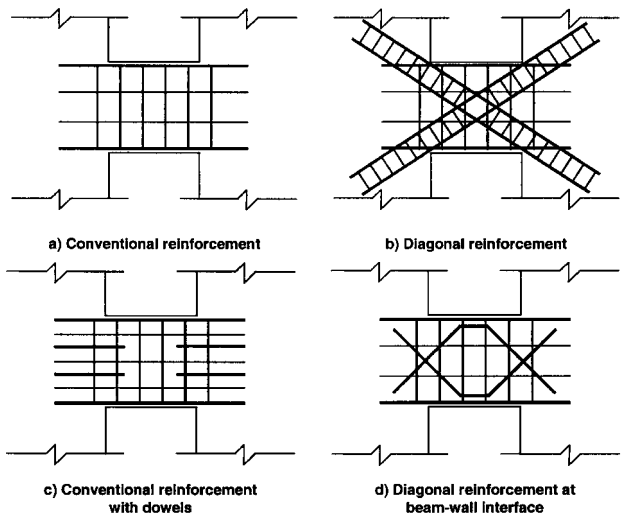

Fig. 1—Reinforcement details in reinforced concrete coupling beams.

ACI Structural Journal, V. 102, No. 1, January-February 2005.
MS No. 04-006 received January 15, 2004, and reviewed under Institute publication policies. Copyright © 2005, American Concrete Institute. All rights reserved, including the making of copies unless permission is obtained from the copyright proprietors. Pertinent discussion including authors' closure, if any, will be published in the November-December 2005 *ACI Structural Journal* if the discussion is received by July 1, 2005.

ACI member **B. Afsin Canbolat** *is a PhD candidate at the University of Michigan, Ann Arbor, Mich. He received his BS from Middle East Technical University, Ankara, Turkey, in 1998, and his MS from the University of Michigan in 2000. His research interests include the seismic behavior and structural applications of high-performance fiber-reinforced cementitious composites.*

ACI member **Gustavo J. Parra-Montesinos** *is an assistant professor at the University of Michigan. He is Secretary of ACI Committee 335, Composite and Hybrid Structures, and is a member of Joint ACI-ASCE Committee 352, Joints and Connections in Monolithic Concrete Structures. His research interests include the seismic behavior and design of reinforced concrete, fiber-reinforced concrete, and hybrid steel-concrete members and structures.*

James K. Wight, *FACI, is a professor of civil engineering at the University of Michigan. He is Chair of ACI Committee 318, Structural Concrete Building Code, and former Chair of ACI Subcommittee 318-E, Shear and Torsion. He is also a member of Joint ACI-ASCE Committees 352, Joints and Connections in Monolithic Concrete Structures, and 445, Shear and Torsion. His research interests include earthquake-resistant design of reinforced concrete structures and the use of high-performance fiber-reinforced cementitious composites in critical members or regions of such structures.*

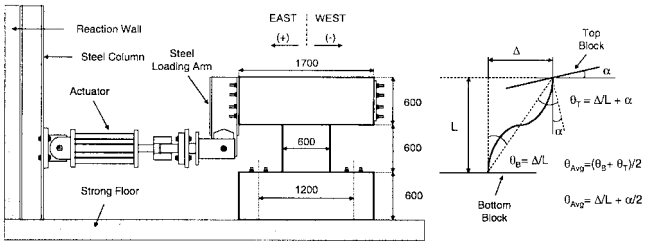

Fig. 2—Dimensions of coupling beam and test setup (mm).

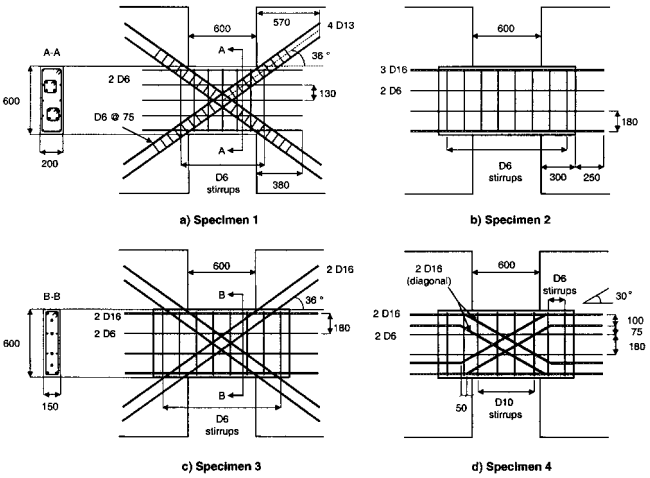

Fig. 3—Reinforcement details of test specimens (dimensions in mm. Concrete cover = 40 and 35 mm for reinforced concrete and high-performance fiber-reinforced cement composite specimens, respectively).

multiple cracking in the composite material. Localization of damage in high-performance fiber-reinforced cement composites (HPFRCCs) is typically observed after crack saturation occurs and at tensile strains ranging between 2.0 and 5.0% (Naaman and Reinhardt 1996). In previous studies on the behavior of HPFRCC members under reversed cyclic loading, it has been reported that the use of these advanced materials leads to significantly higher shear deformation capacity with superior damage tolerance compared with RC members (Parra-Montesinos and Wight 2000; Billington and Yoon 2002; Kim and Parra-Montesinos 2003). Therefore, HPFRCC materials are now considered a serious alternative for use in RC members, particularly those with shear dominant behavior.

The purpose of this research project was to explore the use of HPFRCC materials as a new design alternative in coupling beams. The tension strain-hardening behavior with multiple cracking exhibited by these materials was expected to reduce the dependence on heavily reinforced diagonal cages while maintaining similar strength and ductility compared with well detailed diagonally reinforced coupling beams.

RESEARCH SIGNIFICANCE

In this research, a new type of coupling beam constructed with high-performance fiber-reinforced cement composites (HPFRCCs) was developed to simplify current reinforcement requirements in RC coupling beams. Through an experimental investigation, it is shown that the superior tensile behavior and damage tolerance of HPFRCC allow a simplification of diagonal reinforcement detailing in RC coupling beams while ensuring a stable seismic behavior. In addition, the results from this research provide valuable information on the overall behavior of HPFRCC members with low shear span-to-depth ratios when subjected to large displacement reversals, widening the range of structural applications of HPFRCC materials.

EXPERIMENTAL PROGRAM

Test specimens

In this experimental investigation, four coupling beam specimens were tested under displacement reversals to evaluate the feasibility of using HPFRCC materials in coupling beams with simplified reinforcement detailing. The main variables investigated were the type of cementitious material used in the coupling beam, fiber type, and reinforcement detailing.

Each specimen consisted of an approximately 3/4-scale coupling beam and two stiff RC members representing structural walls. A span-to-depth ratio equal to 1.0 was selected for the coupling beams to ensure a shear-dominant behavior. As the span-to-depth ratio increases, flexural deformations play a more significant role in the behavior of coupling beams. Therefore, the drift capacities obtained in this investigation could be considered as a lower bound for most practical coupling beam aspect ratios. The dimensions for the test specimens and test setup are shown in Fig. 2.

The first specimen, used as the control specimen, consisted of a reinforced concrete coupling beam with diagonal reinforcement. To evaluate the seismic response of coupling beams designed using modern codes, this specimen was designed and detailed according to the ACI 318 (ACI Committee 318 1999), except for the "one-quarter of the minimum member dimension" requirement for the spacing of transverse reinforcement around the diagonal bars, which was found inappropriate for the selected testing scale. Uniformly distributed horizontal and vertical reinforcement were supplied in ratios representing the code limits to minimize their contribution to the flexural and shear capacity of the coupling beam. Figure 3(a) shows a sketch of the reinforcement details used in Specimen 1. The width of the RC coupling beam was dictated by the width of the intersecting diagonal cage groups. Through careful construction, the beam width was limited to 200 mm (8 in.) to ensure a high shear stress demand on the coupling beam.

In Specimen 2, the precast coupling beam was constructed with a HPFRCC material containing a 2.0% volume fraction of ultra-high molecular weight polyethylene (PE) fibers. Contrary to the first specimen, diagonal reinforcement was eliminated and only uniformly distributed horizontal and vertical reinforcement was provided. Also, because of the elimination of diagonal bars and corresponding hoops, the beam width in Specimen 2 was reduced to 150 mm (6 in.) to

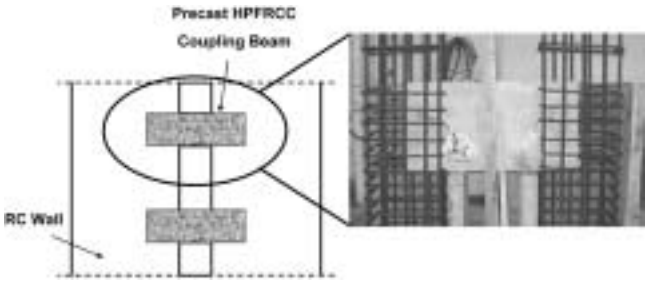

Fig. 4—Use of precast high-performance fiber-reinforced cement composite coupling beams.

increase the shear demand in the composite material. Except for the top and bottom horizontal bars, minimum distributed horizontal and vertical reinforcement was used to evaluate the performance of HPFRCC members under large shear deformations and to investigate the possibility of a total elimination of diagonal reinforcement in coupling beams. The reinforcement details of Specimen 2 are shown in Fig. 3(b).

Because site casting of HPFRCC coupling beams may be difficult for a typical concrete contractor, the use of precast coupling beams was selected as an alternative to cast-in-place beams (Fig. 4). The HPFRCC beams were prefabricated with sufficient embedment length and reinforcement anchorage to ensure proper moment and shear transfer. The construction process started with vertical casting of the walls of the specimen up to the level corresponding to the bottom of the beam, representing the cold joint in real construction. Then, precast coupling beams were placed between the walls, and concrete was cast to encase the ends of the beam and complete the upper portion of the walls. The precast beams were embedded half their span length into each wall to reduce bearing stresses, and the horizontal reinforcing bars were extended beyond the ends of the beam to provide the full development length from the face of the wall (Fig. 3(b) to (d)). This construction process is expected to be practical and attractive for industry because it will not only lead to significant savings in time and workmanship at the site, but also provide good material quality control for the coupling beams.

Specimen 3 had the same type of HPFRCC material as Specimen 2. However, two D16 diagonal bars with no confining reinforcement, corresponding to approximately 80% of the area of diagonal reinforcement used in Specimen 1, were placed in each direction to increase beam displacement and energy dissipation capacity (Fig. 3(c)). The beam width and the amount of distributed horizontal and vertical reinforcement were the same as in Specimen 2, so the contribution of the diagonal bars, which protruded from the precast beam, could be evaluated.

Specimen 4 used the same diagonal bars as Specimen 3. The diagonal reinforcement detailing, however, was modified for easier handling of the precast coupling beams. As shown in Fig. 3(d), the bars ran diagonally within the beam span and were bent at the beam-wall interface so they would stay within the depth of the precast coupling beam. A new composite material, consisting of twisted steel fibers (Naaman 1999) in a 1.5% volume fraction, was used in Specimen 4. Minimum distributed horizontal reinforcement was used, but the distributed vertical reinforcement within the beam span was increased to prevent a premature failure at the bending points of the diagonal bars. The beam width was kept the same as in the other HPFRCC coupling beam

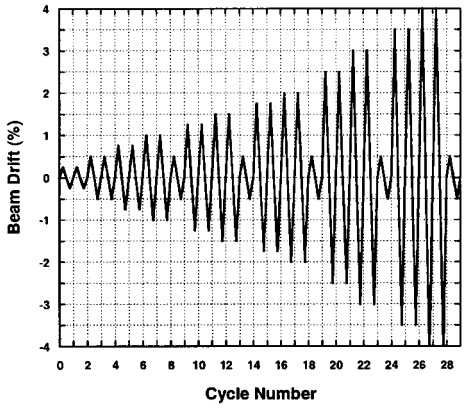

Fig. 5—Intended reversed cyclic displacement pattern.

Table 1—Description of test specimens

Specimen	Diagonal reinforcement	Cement material	Span-to-depth ratio	Horizontal/vertical reinforcement ratio
1	Yes	Concrete	1.0	0.25%/0.25%
2	No	HPFRCC (PE)	1.0	0.25%/0.25%
3	Yes*	HPFRCC (PE)	1.0	0.25%/0.25%
4	Yes*	HPFRCC (twisted steel)	1.0	0.25%/0.60%

*No transverse reinforcement used to confine diagonal bars.

specimens (150 mm). The design parameters and corresponding values are given in Table 1.

Test setup and instrumentation

The test specimens were rotated and placed into the test setup with one of the walls fixed to the strong floor (Fig. 2). In this horizontal position, displacement cycles were applied to the upper wall portion through a horizontal hydraulic actuator with its line of action passing through the midspan of the beam in order to produce an antisymmetrical moment pattern in the coupling beam. The actuator and the upper portion of the specimen were connected through a steel I-section and the load was transferred to the top RC block by means of direct bearing and unbonded threaded bars passing through the top wall. The test specimens were braced laterally to prevent out-of-plane movements.

The specimens were subjected to quasi-static cyclic loading in a displacement control mode, following a predefined reversed cyclic displacement pattern. To simulate the demands during an earthquake, several lateral displacement cycles were applied to each specimen, starting from a coupling beam drift of 0.25%, and reaching a maximum drift of 4% (provided that the specimen did not fail at a lower drift level), as shown in Fig. 5. Each cycle to a given drift level was applied twice to evaluate the loss of strength and stiffness in the specimens during the repeated cycles. Some 0.5% drift cycles were interspersed into the displacement history to evaluate the residual stiffness of the specimens.

The horizontal displacement reached at each drift level was monitored through linear potentiometers because LVDT readings from the hydraulic actuator were inaccurate due to deformations in the loading system. Additional potentiometers were also used to check any rotation of the top wall with respect to the bottom wall. The lateral displacement applied to the specimens was then based on the calculation of a net beam

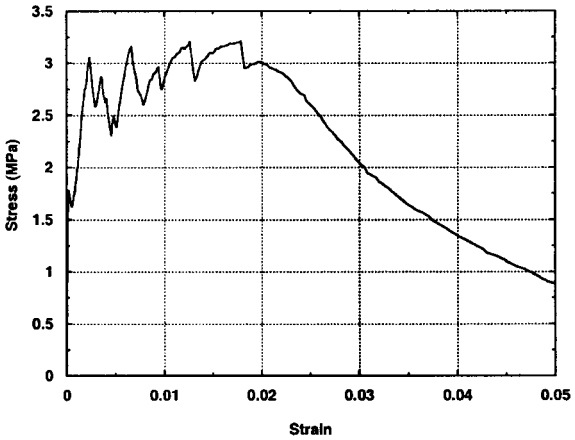

Fig. 6—Typical tensile stress versus strain response of sample specimen with polyethylene fibers.

Table 2—Fiber properties

Fiber type	Material	Test strength, MPa (ksi)	Elastic modulus, GPa (ksi)	Diameter, mm (in.)	Length, mm (in.)	Volume in composite, %
PE	UHMWPE*	2570 (375)	117 (17,000)	0.038 (0.0015)	13 (0.5)	2.0
Twisted steel	Steel	2470 (360)	200 (29,000)	0.3 (0.012)	30 (1.2)	1.5

*Ultra-high molecular weight polyethylene.

drift θ_{Avg} obtained through the potentiometer readings and taking into account the effect of wall rotation on drift (Fig. 2).

One face of the coupling beam was instrumented with potentiometers that were positioned horizontally, vertically, and diagonally to record an average state of strain in the coupling beam. Also, potentiometers were placed at the top and bottom of the beam, adjacent to the walls, to monitor beam rotations in the region near the wall faces. Clinometers, rotation measuring devices, were also used at the beam and wall faces to verify the rotations measured by the potentiometers. Strains in the steel reinforcing bars were monitored through strain gauges attached to the surface of the bars at various locations.

Material testing and development

Fiber-reinforced concrete is not a new material, but recent improvements in material tensile properties and ductility, development of polymer-based and high-strength steel fibers, and optimization of cementitious composites have led to new research on the behavior of HPFRCC materials under extreme loading conditions. Findings from experimental studies have indicated that HPFRCC can exhibit a ductile response in tension similar to strain hardening behavior of metals (Li 1993). In plain concrete, the first crack formation results in a rapid loss of tensile strength. In fiber cementitious composites with strain hardening response, however, fibers bridging initial tension cracks carry an increasing amount of force across these cracks, leading to the formation of multiple cracks in the composite. This crack formation process continues, while maintaining tensile strength, until the peak bridging stress is reached on one of the cracks, leading to a wide opening of that crack. At higher deformations, damage is localized on this particular crack and the composite tensile strength diminishes gradually. In the end, a highly ductile tensile performance is achieved with a multiple cracking pattern and significant damage tolerance. Achieving this tensile performance is primarily related to the volume fraction of the fibers in the composite, fiber material and geometry, cementitious matrix composition, average bond strength at the fiber-matrix interface, and homogeneous distribution of fibers in the matrix.

In this research study, different mixture proportions were considered for use in the coupling beams and several tension and compression specimens were tested to obtain the desired performance in the composite. Dogbone-shaped specimens of two different sizes were used for uniaxial tension tests. Small dogbone specimens tested in this investigation had a cross section of 25 x 25 mm (1 x 1 in.) with a length of 215 mm (8.5 in.). Large dogbone specimens were also tested to evaluate size effect. To keep the same cross-sectional area, the specimen dimensions were selected to be 12.5 x 50 mm (0.5 x 2 in.) in cross section and 560 mm (22 in.) in length.

From the trial mixture proportions, two FRC composites with the desired multiple cracking behavior in tension were produced using a 2.0% volume fraction of PE fibers and a 1.5% volume fraction of twisted steel fibers. PE fibers are made of an ultra-high molecular weight polyethylene, widely used in fiber-reinforced polymers for the aerospace industry. Twisted steel fibers have superior frictional and mechanical bond properties, compared with commercially available steel fibers (Naaman 1999). Table 2 lists the properties of the PE and twisted steel fibers used in this research.

The compressive strength values at the test day were approximately 57 and 63 MPa (8300 and 9100 psi), and the postcracking tensile strengths were approximately 3.1 and 5.5 MPa (450 and 8000 psi) for the composites with PE and twisted steel fibers, respectively. A typical tensile stress versus strain response obtained from a small dogbone specimen with PE fibers is shown in Fig. 6. It has been experimentally shown that the monotonic tensile behavior of HPFRCC represents an envelope of tensile response under reversed cyclic loading, given that the strain at peak compressive strength is not exceeded during reversed cyclic loading (Kesner, Billington, and Douglas 2003).

Regular concrete, provided by a local concrete supplier, was used in the coupling beam of the first specimen and in the walls of all the specimens. The compressive strength measured for the concrete used in Specimen 1 on the test day was approximately 41 MPa (6000 psi). All the deformed steel reinforcement used in this study was Grade 60 (420 MPa). Tensile test results from the steel supplier, confirmed by tensile tests conducted at the University of Michigan, indicated a yield stress of 450 MPa (65 ksi) and a tensile strength of 726 MPa (105 ksi).

EVALUATION OF EXPERIMENTAL RESULTS

A predefined displacement history (Fig. 5) with several cycles to drift levels ranging from 0.25% up to a maximum of 4.0% was intended to be applied to the specimens. The test setup was configured to develop a contraflexure moment diagram in the coupling beam, and no constraints were built to prevent a rotation of the top block. Due to rotations of the top block, the intended drift levels did not always correspond to the actual drifts experienced by the coupling beams. Thus, the drifts in the coupling beams due to lateral displacements (displacement ÷ coupling beam length) were adjusted to account for the differential rotation between the top and bottom blocks that simulated the coupled walls (Fig. 2). The drift levels referred to in the following are the adjusted drift values.

Key experimental results for all test specimens, including maximum shear force, drift capacity, and peak shear stresses, are given in Table 3. Drift capacity was determined as the maximum drift level before a strength loss of 20% or more was observed.

Shear force beam drift response

The shear force versus drift response of Specimen 1 is shown in Fig. 7(a). The behavior observed in this specimen indicated that diagonally reinforced RC coupling beams designed according to the ACI Building Code exhibit a stable behavior under high shear and deformation demands. At up to a 0.5% drift level, the RC coupling beam remained elastic. At larger drifts, yielding of the diagonal reinforcing bars led to wide hysteresis loops with excellent energy dissipation capacity. The maximum force applied to Specimen 1 was approximately 470 kN (105 kips), which corresponded to a shear stress level of 3.8 MPa (550 psi). For this particular specimen, the concrete compressive strength was 41 MPa (6000 psi), and thus the maximum applied shear stress was equivalent to $0.6\sqrt{f'_c}$ MPa ($7.1\sqrt{f'_c}$ psi). The shear strength provided by the diagonal reinforcement in Specimen 1, acting at a stress of 450 MPa (65 ksi), was approximately 270 kN (60 kips). It is likely, however, that this contribution increased significantly during the later drift cycles due to strain hardening of the steel reinforcement. Throughout the test, no indication of buckling or anchorage problems in the diagonal bars was observed.

Specimen 2 was constructed with PE fibers at a 2.0% volume fraction. To evaluate the effectiveness of this material to provide diagonal tension strength and adequate displacement capacity in coupling beams, no diagonal reinforcement was used in this specimen. As shown in Fig. 7(b), Specimen 2 exhibited a stable response up to 2.0% drift, where a significant drop in beam strength was observed due to fiber pullout. The hysteresis loops showed some pinching with less energy dissipation capacity compared with Specimen 1. This pinching is due to the fact that the polyethylene fibers are effective in restraining crack opening, but once unloaded, they do not provide any resistance against crack closing. Thus, force transfer across cracks during the crack closing process was a function of the distributed horizontal and vertical reinforcement crossing the cracks.

In terms of shear strength, Specimen 2 sustained a demand of approximately 6.2 MPa (900 psi), which was 60% larger than that in Specimen 1. This applied shear stress corresponded to $0.8\sqrt{f'_c}$ MPa ($10\sqrt{f'_c}$ psi), given that the compressive strength of the HPFRCC material used in this specimen was approximately 57 MPa (8300 psi). The shear strength provided by the HPFRCC material was calculated based on the diagonal tension strength provided by the fibers bridging a diagonal crack spanning from one corner of the coupling beam to the other corner. From the postcracking tensile strength of 3.1 MPa (450 psi) obtained for the HPFRCC material used in Specimen 2, a shear strength contribution of 290 kN (65 kips) was estimated, which represents half of the strength observed in Specimen 2. This estimated fiber strength contribution is consistent with the observed strength loss that occurred when the major diagonal cracks formed after 2.0% drift.

Specimen 3 had cementitious composite and distributed reinforcement properties similar to those used in Specimen 2. Two diagonal bars in each direction, without confinement steel, were added to evaluate their potential for increasing the energy dissipation and drift capacity of HPFRCC coupling beams. The shear force versus drift response shown in Fig. 7(c) indicated that the supplemental diagonal bars led to a significant increase in the strength and displacement capacity of the coupling beam. In terms of strength, the diagonal bars were estimated to contribute approximately 210 kN (47 kips) of shear strength (26% of maximum beam strength) at a yield stress of 450 MPa (65 ksi). Consistent with this expected strength, the difference in strength between Specimens 2 and 3 was approximately 200 kN (45 kips). The maximum load of 800 kN (180 kips) was recorded in Specimen 3 at approximately 2.5% drift. This peak load was maintained up to 4% drift in the positive direction, where a sudden drop of approximately 290 kN (65 kips) was observed due to the loss of diagonal tension strength in the HPFRCC material. During subsequent loading cycles, the residual shear strength was below 450 kN (100 kips), and was primarily due to the shear-carrying capacity provided by the diagonal bars and transverse reinforcement. After the major diagonal cracks opened widely, the fiber cementitious material began losing its ability to support the diagonal bars. During the repeated cycle in the negative direction targeted to 4.0% drift, the diagonal bars under compression buckled, losing their load carrying capacity.

With regard to displacement capacity, a maximum drift of approximately 4.0% was reached in Specimen 3, which is almost twice that of Specimen 2. It should be noted that extensive rotations in the top block affected the applied displacement history. As can be observed in Fig. 7(c), the adjusted drift levels reached in the positive loading direction

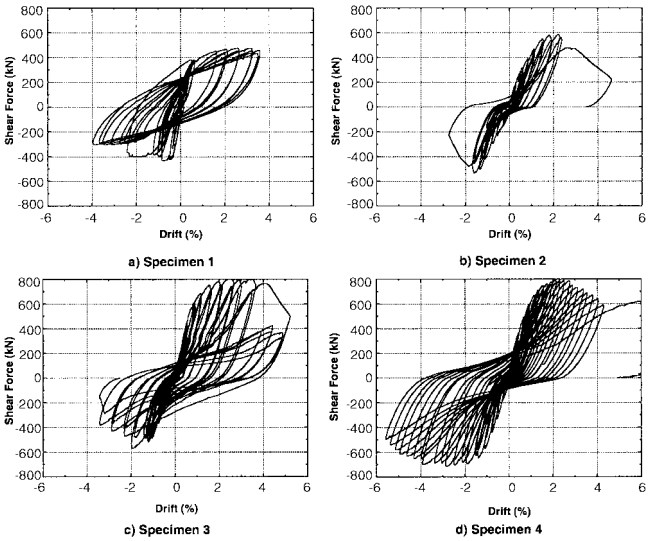

Fig. 7—Shear force versus beam drift response.

Table 3—Summary of experimental results

Specimen	P_{MAX}, kN (kips)	Drift capacity, %	Shear stress, MPa (psi)	Shear stress ($\sqrt{f'_c}$), MPa (psi)
1	470 (105)	4.0*	3.8 (550)	0.6 (7.1)
2	600 (135)	1.8	6.2 (900)	0.8 (10)
3	800 (180)	4.0	8.6 (1250)	1.15 (14)
4	800 (180)	4.0	8.6 (1250)	1.1 (13)

*No clear indication of failure was observed in Specimen 1.

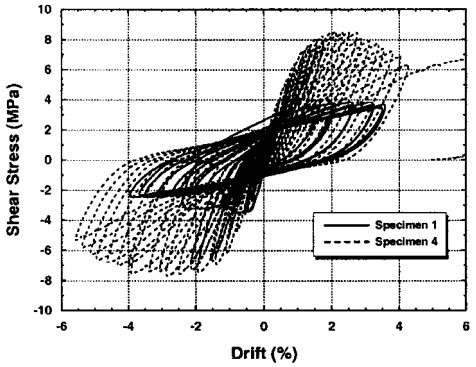

Fig. 8—Shear stress versus drift response of Specimens 1 and 4.

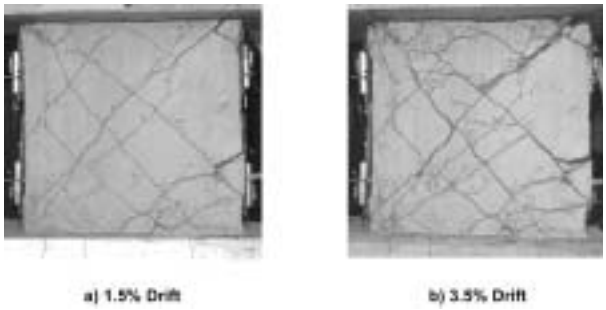

Fig. 9—Cracking pattern in Specimen 1.

in Specimen 3 were larger than those in the negative loading direction. The shape of the hysteresis loops indicated that the energy dissipation capacity of Specimen 3 was significantly larger than that of Specimen 2.

The maximum average shear stress in Specimen 3 was 8.6 MPa (1250 psi), which represented 230% of the peak shear stress measured in Specimen 1. Evaluating this strength in terms of the square root of the cement composite compressive strength, it represented $1.15\sqrt{f'_c}$ MPa ($14\sqrt{f'_c}$ psi), which is 40% larger than the maximum shear stress allowed in the ACI 318 Code (ACI Committee 318 1999).

Contrary to the straight diagonal bars used in Specimen 3, those in Specimen 4 were bent near the beam-wall interface to facilitate the construction process for a precast beam, as shown in Fig. 3(d). In addition to the variation in reinforcement details, twisted steel fibers in a 1.5% volume fraction were used in this specimen. The predefined cyclic displacement pattern was slightly modified for this specimen. As can be seen in Fig. 5, the drift pattern used in the previous specimens consisted of repeated cycles to a 0.5% larger drift after 2.0% drift. In Specimen 4, single cycles were incremented by 0.25% for drifts larger than 2.0%, representing a more gradual increase in drift values. With this modification in the displacement history, it was intended to better evaluate the drift level at fiber pullout. In addition to that, when a target displacement was reached, the displacement was not held constant to mark cracks, but the specimen was unloaded to prevent a sudden energy release due to fiber pullout. The shear force versus drift response given in Fig. 7(d) demonstrated that Specimen 4 had a very stable response with good energy dissipation, comparable to Specimen 3. Further, it can be observed that the bent diagonal bars performed as well as the straight bars used in Specimen 3.

In terms of peak strength of Specimen 4, a maximum load of approximately 800 kN (180 kips), similar to that of

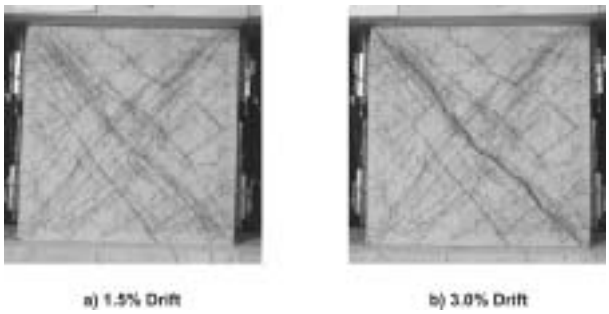

Fig 10—Cracking pattern in Specimen 2.

Specimen 3, was measured at a drift of 2.0%. After this drift level, the contribution of the fiber cementitious material to coupling beam strength started to deteriorate due to the decrease in tensile strength of the HPFRCC with twisted steel fibers. However, the strains in the diagonal bars were large enough to cause these bars to go into strain hardening, increasing reinforcement contribution to shear strength and leading to a gradual decrease in beam shear strength up to 4.0% drift. Specimen 4 was displaced up to 5.5% drift in the negative loading direction with a corresponding applied shear of approximately 70% of the peak load in that direction. At the end of the test, the specimen was displaced monotonically in the positive loading direction up to nearly 8.0% drift, at which point the diagonal bars fractured. The load measured at this drift level was approximately 80% of the peak load for that loading direction, indicating that the cementitious material was effective in supporting the diagonal bars even after opening of wide diagonal cracks. Because the peak strength measured in Specimen 4 was approximately the same as that in Specimen 3, the shear stress demand was also 8.6 MPa (1250 psi). This shear stress translated into $1.1\sqrt{f'_c}$ MPa ($13\sqrt{f'_c}$ psi), which is also significantly larger than the maximum allowable shear stress in the ACI 318 Code (ACI Committee 318 1999) for a coupling beam.

A comparison between the shear stress versus drift response for Specimens 1 and 4 is shown in Fig. 8. Compared with the control Specimen 1, Specimen 4 sustained shear stresses twice as large and possessed substantially larger energy dissipation capacity.

Cracking pattern and damage progress

In Specimen 1, diagonal cracks were first observed during the cycles to 0.25% drift. At 1.5% drift, diagonal cracks widened up to 3 mm (0.12 in.), and beam damage could be classified as moderate (Fig. 9(a)). At drift levels larger than 2.5%, damage became severe with diagonal cracks 5 mm (0.2 in.) wide, concrete spalling, and tensile strains in the diagonal reinforcement in excess of 1.5%. Figure 9(b) shows the extent of damage in Specimen 1 at 3.5% drift. Even though extensive cracking and damage had occurred at the maximum drift level of 4.0%, no clear indication of failure was observed.

Diagonal cracks in Specimen 2 started to form during the cycles to 0.25% drift. As the test progressed, several diagonal cracks propagated throughout the beam, as opposed to only a few diagonal cracks in Specimen 1, with regular concrete. At 1.5% drift, the coupling beam was crossed by tens of diagonal cracks, mostly with a width narrower than 1 mm (0.04 in.) (Fig. 10(a)). However, signs of damage localization were also noticed at this drift level in the negative loading direction as one diagonal crack, which extended

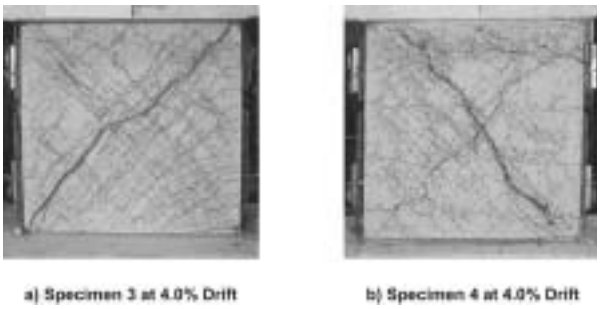

Fig. 11—Cracking pattern in Specimens 3 and 4.

from corner to corner of the coupling beam, began to open as wide as 4 mm (0.16 in.). Also, yielding of the main longitudinal reinforcement of the coupling beam occurred at the beam-wall interface. When the specimen was displaced further, fiber pullout occurred, leading to the opening of a wide diagonal crack (Fig. 10(b)) with a subsequent drop in the strength of the coupling beam. When the displacement was reversed, another diagonal crack, perpendicular to the previously formed crack, opened widely and resulted in a diagonal tension failure of the coupling beam.

A damage progress similar to that of Specimen 2 was observed in Specimen 3. Diagonal cracking began during the cycles to 0.25% drift and a large number of hairline cracks with widths ranging between 0.3 to 0.75 mm (0.01 to 0.03 in.) had formed when the 1.5% drift level was reached. At approximately 2.0% drift, damage localization initiated at a few diagonal cracks that spanned opposite corners in the coupling beam. Contrary to the behavior of Specimen 2, however, Specimen 3 carried increasing amounts of load at drifts up to 4.0% due to the use of supplementary diagonal reinforcement (Fig. 11(a)).

The first diagonal cracks in Specimen 4 were also observed at 0.25% drift and a multiple diagonal cracking pattern formed as the test continued. At approximately 2.0% drift, yielding of the diagonal bars was first noticed and the largest crack width was approximately 1 mm (0.04 in.). As the specimen was pushed to larger drifts, damage localization began with the opening of a few wide diagonal cracks. Figure 11(b) shows the opening of a diagonal crack at 4.0% drift in the negative loading direction. As mentioned previously, Specimen 4 was displaced monotonically in the positive loading direction up to nearly 8.0% drift at the end of the test. As a result, the coupling beam failed due to fracture of the diagonal bars associated with wide diagonal cracks.

Shear distortion response

The shear distortions in the test specimens were calculated by using the record of six displacement transducers placed on one face of the beam that measured deformations in the vertical, horizontal, and diagonal directions. Figure 12 shows the shear force versus shear distortion response for the four coupling beams tested in this investigation. Specimen 1, detailed as per the 1999 ACI 318 Code, exhibited a stable shear response throughout the test (Fig. 12(a)). Because the diagonal bars resisted most of the applied shear force, wide hysteresis loops were obtained. It should be noted that the maximum shear distortion measured in Specimen 1 was 1.5% (0.015 rad). If this distortion is compared with the maximum applied drift of approximately 4.0%, it is clear that flexural deformations played a significant role in the behavior of Specimen 1.

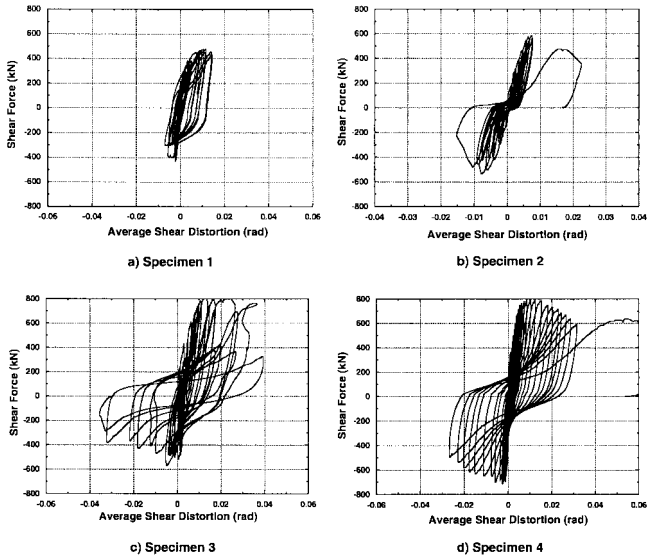

Fig. 12—Shear force versus shear distortion response.

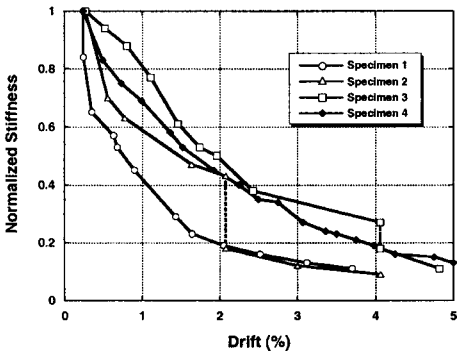

Fig. 13—Normalized stiffness versus beam drift response.

In Specimen 2, with PE fibers and no diagonal bars, a shear force versus distortion response with significant pinching was obtained, as shown in Fig. 12(b). As explained previously, this pinched behavior occurred because the PE fibers are only effective in transferring tensile forces between diagonal cracks. When the displacement (load) direction was reversed, the fibers did not resist the crack closing process, and thus only the steel reinforcement crossing the cracks contributed transfer forces across cracks. Once the diagonal cracks closed, the specimen regained its stiffness. From Fig. 12(b), it was observed that the coupling beam in Specimen 2 had a shear distortion capacity of approximately 1.0%. At this distortion level, fiber pullout occurred, leading to a significant drop in the strength of the specimen.

Compared with Specimen 2, the use of diagonal bars in Specimens 3 and 4 led to a significant improvement in shear distortion capacity. Specimen 3 sustained a shear distortion of approximately 2.5% in the positive loading direction before a significant drop in strength occurred (Fig. 12(c)). This large distortion, compared with Specimen 1, also indicates that shear deformations played a dominant role in the specimen response. In Specimen 4 with twisted steel fibers, a strength decay began before a 2.0% shear distortion as the fibers began pulling out (Fig. 12(d)). However, because of the increasing strength contribution of the diagonal bars as they strain hardened, the loss of shear strength was gradual. In this specimen, a maximum shear distortion of 3.0% was measured during the cycles to approximately 4.0 to 5.0% drift. During

the final push, a shear distortion of 6.0% was measured just before fracture of the diagonal reinforcement occurred.

In all three specimens constructed with a fiber cementitious material, only minor damage was observed at shear distortions of up to 1.0%. When diagonal reinforcement was provided to prevent a sudden failure after fiber pullout, a 1.5 to 2.0% shear distortion could be considered the limit for moderate damage. For larger shear distortions, damage localization with significant crack opening due to fiber pullout can be expected.

Stiffness retention

Stiffness degradation in all four specimens was evaluated by means of the secant stiffness, measured from peak-to-peak displacement point in each direction. To account for the variations in specimen parameters, such as different specimen widths and lack of coarse aggregate in the fiber-reinforced composites, stiffness values were normalized with respect to the secant stiffness at 0.25% drift for each specimen. The normalized stiffness versus drift response shown in Fig. 13 indicates that HPFRCC coupling beams are able to better maintain their stiffness compared with diagonally reinforced RC coupling beams. Initial crack formation in Specimen 1 caused significant stiffness drops during the early cycles. HPFRCC specimens, on the other hand, show a relatively gradual stiffness decrease up to at least 2.0% drift. At that point in Specimen 2, the opening of a large diagonal crack caused a sudden stiffness drop. The presence of diagonal reinforcement in Specimen 3 not only delayed this stiffness drop up to 4.0% drift, but also improved the stiffness retention at low drift values. When the normalized stiffness values at 2.0% drift for the four specimens are compared, it can be seen that Specimen 1 maintained only 20% of its initial stiffness, whereas the fiber-reinforced composite specimens maintained approximately 40 to 50% of their initial stiffness, demonstrating the superior stiffness retention capacity of the HPFRCC coupling beams.

SUMMARY AND CONCLUSIONS

To simplify the reinforcement requirements in diagonally reinforced RC coupling beams, an alternative design consisting of precast HPFRCC coupling beams with different reinforcement configurations was experimentally investigated. The reinforcement details evaluated in this research project included the use of only distributed horizontal and vertical reinforcement and the use of supplementary diagonal bars without transverse steel reinforcement. The first specimen, used as the control specimen, consisted of an RC coupling beam with diagonal reinforcement designed and detailed according to the ACI 318 Code. In the second specimen, the coupling beam was constructed with a HPFRCC containing PE fibers, and only conventional horizontal and vertical reinforcement was provided. Specimens 3 and 4 were constructed with HPFRCC containing PE and twisted steel fibers, respectively, and supplementary diagonal reinforcement, but no confinement hoops were provided.

The structural performance of these new precast HPFRCC coupling beams under reversed cyclic loading demonstrated that a more convenient reinforcement detailing can be used in coupling beams and still maintain adequate seismic behavior. The use of advanced fiber cementitious materials allowed the elimination of the transverse reinforcement typically required around the diagonal bars for confinement, thus simplifying the beam construction process. The test results showed that HPFRCC coupling beams with simplified diagonal reinforcement exhibited higher shear strength and stiffness retention. HPFRCC beams with supplemental diagonal bars reached a drift of at least 4.0% while maintaining approximately 80% of their shear-carrying capacity. Considering the multiple cracking pattern with hairline diagonal cracks up to fiber pullout experienced by the HPFRCC coupling beams, it is clear that HPFRCC materials have superior damage tolerance under large displacement reversals compared with regular concrete.

ACKNOWLEDGMENTS

The research study described herein was sponsored by the National Science Foundation under the Grant No. CMS 0001617. The opinions expressed in this paper are those of the authors and do not necessarily reflect the views of the sponsor. The twisted steel fibers used in this study were specially fabricated by Sodetal, France, for Professor Antoine E. Naaman.

REFERENCES

ACI Committee 318, 1999, "Building Code Requirements for Structural Concrete (ACI 318-99) and Commentary (ACI 318R-99)," American Concrete Institute, Farmington Hills, Mich., 392 pp.

ACI Committee 318, 2002, "Building Code Requirements for Structural Concrete (ACI 318-02) and Commentary (ACI 318R-02)," American Concrete Institute, Farmington Hills, Mich., 443 pp.

American Iron and Steel Institute, 1975, *Earthquakes*, pp. 160-161.

Billington, S. L., and Yoon, J., 2002, "Cyclic Behavior of Precast Post-Tensioned Segmental Concrete Columns with ECC," *Proceedings of the JCI International Workshop on Ductile Fiber Reinforced Cementitious Composites (DFRCC)—Applications and Evaluation (DFRCC-2002)*, Japan Concrete Institute, Tokyo, Oct., pp. 279-288.

Galano, L., and Vignoli, A., 2000, "Seismic Behavior of Short Coupling Beams with Different Reinforcement Layouts," *ACI Structural Journal*, V. 97, No. 6, Nov.-Dec., pp. 876-885.

Kesner, K. E.; Billington, S. L.; and Douglas, K. S., 2003, "Cyclic Response of Highly Ductile Fiber-Reinforced Cement-Based Composites," *ACI Materials Journal*, V. 100, No. 5, Sept.-Oct., pp. 381-391.

Kim, K., and Parra-Montesinos, G. J., 2003, "Behavior of HPFRCC Low-Rise Walls Subjected to Displacement Reversals," *High Performance Fiber Reinforced Cement Composites 4 (HPFRCC 4)*, Proceedings of the Fourth International RILEM Workshop, A. E. Naaman and H. W. Reinhardt, eds., RILEM Publications, s.a.r.l., Cachan Cedex, France, pp. 505-515.

Li, V. C., 1993, "From Micromechanics to Structural Engineering—The Design of Cementitious Composites for Civil Engineering Applications," *Journal of Structural Mechanics and Earthquake Engineering*, JSCE, V. 10, No. 2, pp. 37-48.

Luisoni, C. J.; Somenson, H. M.; and Ungaro, M. A., "Verificación Experimental de un Cálculo Plástico y Otro Elástico do una Patred de Corte," *IV Simposio Panamericano de Estructuras*, V. 5, Oct. 1970, pp. 230-286. (in Spanish)

Naaman, A. E., 1999, "Fibers with Slip Hardening Bond," *High Performance Fiber Reinforced Cement Composites 3 (HPFRCC 3)*, Proceedings of the Third International RILEM Workshop, H. W. Reinhardt and A. E. Naaman, eds., RILEM Publications, s.a.r.l., Cachan Cedex, France, pp. 371-385.

Naaman, A. E., and Reinhardt, H. W., 1996, "Characterization of High Performance Fiber Reinforced Cement Composites—HPFRCC," *High Performance Fiber Reinforced Cement Composites 2 (HPFRCC 2)*, Proceedings of the Second International RILEM Workshop, A. E. Naaman and H. W. Reinhardt, eds., RILEM Publications, s.a.r.l., Cachan Cedex, France, pp. 1-24.

Parra-Montesinos, G. J., and Wight, J. K., 2000, "Seismic Response of Exterior RC Column-to-Steel Beam Connections," *Journal of Structural Engineering*, ASCE, V. 126, No. 10, pp. 1113-1121.

Paulay, T., and Binney, J. R., 1974, "Diagonally Reinforced Coupling Beams of Shear Walls," *Shear in Reinforced Concrete*, SP-42, V. 2, American Concrete Institute, Farmington Hills, Mich., pp. 579-598.

Paulay, T., and Santhakumar, A. R., 1976, "Ductile Behavior of Coupled Shear Walls," *Journal of the Structural Division*, ASCE, V. 102, pp. 93-108.

Shiu, N. K.; Barney, G. B.; Fiorato, A. E.; and Corley W. G., 1978, "Revering Load Tests of Reinforced Concrete Coupling Beams," *Proceedings of the Central American Conference on Earthquake Engineering*, El Salvador, pp. 239-249.

Tassios, T. P.; Moretti, M.; and Bezas A., 1996, "On the Behavior and Ductility of Reinforced Concrete Coupling Beams of Shear Walls," *ACI Structural Journal*, V. 93, No. 6, Nov.-Dec., pp. 711-720.